

Formation of bound composite vortices of a singly-quantized 1S_0 vortex and half-quantized 3P_2 vortices in the 1S_0 - 3P_2 coexisting phase in neutron stars

Tatsuhiko Hattori,^{1,*} Muneto Nitta,^{2,3,†} and Kazuyuki Sekizawa^{1,4,5,‡}

¹*Department of Physics, School of Science, Institute of Science Tokyo, Tokyo 152-8550, Japan*

²*Department of Physics & Research and Education Center for Natural Sciences, Keio University, 4-1-1 Hiyoshi, Yokohama, Kanagawa 223-8521, Japan*

³*International Institute for Sustainability with Knotted Chiral Meta Matter (WPI-SKCM²), Hiroshima University, 1-3-1 Kagamiyama, Higashi-Hiroshima, Hiroshima 739-8531, Japan*

⁴*Nuclear Physics Division, Center for Computational Sciences, University of Tsukuba, Ibaraki 305-8577, Japan*

⁵*RIKEN Nishina Center, Saitama 351-0198, Japan*

(Dated: May 28, 2026)

Background: Pulsar glitches are believed to originate from the dynamics of quantized vortices in the neutron superfluid interior. The outer core of a neutron star hosts 3P_2 spin-triplet superfluid, whose half-quantized vortices (HQVs) are qualitatively different from 1S_0 singly-quantized vortices (SQVs) in the inner crust. It has recently been proposed that the coupling between these two vortex species gives rise to a large-scale vortex network, providing a candidate mechanism for the diversity of observed pulsar glitch phenomena.

Purpose: We aim to elucidate the effect of interaction between a SQV in the 1S_0 neutron superfluid and HQVs in the 3P_2 neutron superfluid, which may be important near the crust-core boundary, where those two phases may coexist.

Methods: Using the Gross–Pitaevskii equations for the usual 1S_0 BEC and 3P_2 spinor BEC, we perform two-dimensional simulations of one 1S_0 SQV and two 3P_2 HQVs in a coexistence phase, varying the density–density and Josephson coupling constants.

Results: We perform two-dimensional calculations for the 1S_0 - 3P_2 coexisting phase with varying the magnitude of the coupling constants density–density as well as Josephson coupling terms. From the results, we find that the Josephson term, arising from the relative phase between the 1S_0 and 3P_2 condensates, induces a strong attractive interaction between the two HQVs and the single SQV, which dominates over the density–density coupling term. When pinning potentials are applied to the 3P_2 HQVs and the 1S_0 SQV at spatially separated locations, the Josephson-term-driven attraction is found to be sufficiently strong to overcome the pinning potential and drive vortex depinning, demonstrating that the inter-condensate phase coupling can significantly alter the spatial configuration of quantized vortices near the phase boundary.

Conclusions: These results demonstrate that the Josephson coupling plays an important role in the HQV–SQV interaction, and suggest that two HQVs and one SQV can form a bound composite vortex at the phase boundary between the inner crust and the outer core of neutron stars.

I. INTRODUCTION

Neutron stars are among the densest objects in the universe, with central densities exceeding nuclear saturation density [1], making them a unique laboratory at the intersection of particle physics, nuclear physics, and astrophysics. Formed as the compact remnants of core-collapse supernovae, neutron stars rotate rapidly, with spin periods ranging from approximately 1 ms to ~ 10 s [2]. A subset of neutron stars emit beams of electromagnetic radiation from their magnetic poles; because this emission is observed as periodic pulses synchronized with the rotation, these objects are known as *pulsars* [1]. The interior of a neutron star reaches densities far exceeding those achievable in terrestrial nuclear experiments, making it the only known realization of cold, supranuclear-density matter in the universe [1,3].

Among the observable properties of pulsars, the mass and spin period can be measured with exceptional precision via

radio or X-ray timing [2]. In contrast, the radius has remained difficult to constrain and has only recently been measured to meaningful precision, primarily through X-ray pulse-profile modeling by the Neutron Star Interior Composition Explorer (NICER) [4,5]. The magnetic field strength and its internal configuration remain subject to considerable observational uncertainty. Thermal X-ray observations of neutron star surfaces provide an additional window into the stellar interior: the rapid cooling of the neutron star in Cassiopeia A, observed in real time by the *Chandra* X-ray Observatory, has been interpreted as direct evidence for the onset of 3P_2 neutron superfluidity in the stellar core [6,7]. This represents the first observational indication that superfluidity and superconductivity occur at nuclear densities inside neutron stars, see [2,8–10] as a review for superfluidity. Furthermore, the frictional motion of pinned superfluid vortices during spin-down — known as vortex creep — has been proposed as an internal heating mechanism that may explain the unexpectedly high surface temperatures of old neutron stars [11–13], connecting vortex dynamics to neutron star thermal observations.

A hallmark observational phenomenon associated with neutron stars is the *glitch* [14,15], a sudden, quasi-periodic spin-up of the pulsar rotation frequency [16,17]. The glitch

* hattori.t.a850@m.isct.ac.jp

† mune.nitta@gmail.com

‡ sekizawa@phys.sci.isct.ac.jp

mechanism is widely believed to involve the dynamics of quantized vortices in the neutron superfluid interior. The conventional avalanche model attributes glitches to the sudden unpinning of 1S_0 superfluid vortices in the inner crust see, e.g., Refs. [11,18–29], and references therein. However, a growing number of observations have revealed glitch events that cannot be accounted for by this model [30,31], calling for a new theoretical framework that can describe the full diversity of observed glitch phenomena.

In the outer core of a neutron star, neutrons are expected to form a 3P_2 superfluid [32–49], a spin-triplet p -wave condensate that is realized in only a handful of systems on Earth, such as ^3He superfluid. Moreover, the outer core hosts a coexistence of neutron superfluidity and proton superconductivity, rendering it a rare example of a multi-component condensate system of broad interest to condensed matter physics. On the theoretical side, significant progress has been made in the microscopic understanding of the 3P_2 superfluid. The Ginzburg-Landau (GL) framework [49–53] enables us to study the ground states and nonuniform states such as vortices. The ground state is a nematic phase [50], and more precisely it is in the uniaxial (UN), D_2 biaxial nematic (D_2 -BN), or D_4 biaxial nematic (D_4 -BN) phase depending on the strength of magnetic fields and temperature [51–53]. Vortices in the 3P_2 superfluids have been studied in the GL framework [51,54–59]; As a result of internal degrees of freedom, the 3P_2 superfluids allow half-quantized vortices (HQVs) in a strong magnetic field in which the phase is in the D_4 -BN [56]. These vortices are also characterized by the non-Abelian fundamental group and are called non-Abelian HQVs. A singly quantized vortex (SQV) is split into two HQVs forming a vortex molecule structure [58], and the interaction between two or more molecules was studied [59]. Other than vortices domain walls [60] and surface defects [61] were also studied. There are also rich massless and massive bosonic excitations [62–74], which were proposed to explain cooling and transport phenomena in neutron stars.

Moreover, recently the 3P_2 superfluids have been studied microscopically by using the Eilenberger and Bogoliubov–de Gennes (BdG) equations [75–77] which are valid in the temperature and can describe short distance behaviours such as vortex cores. The complete phase diagram under a strong magnetic field and temperature and topological superfluidity such as topologically protected gapless Majorana fermions on surfaces and vortex cores were shown. Subsequently, the first microscopic study of quantized vortices in 3P_2 superfluids was made in the BdG equation [78–80]. In particular, a SQV was found to host two zero-energy Majorana fermion bound states in its core [78]. Such a SQV is split into two non-Abelian HQVs [79] consistent with the analysis in the GL theory, and each HQV hosts a single zero-energy Majorana fermion bound state.

Separately, the coexistence of 1S_0 and 3P_2 superfluids was studied within the GL framework [81], obtaining the phase diagram as a function of temperature and magnetic field. They showed that the coupling between the condensates for 1S_0 and 3P_2 superfluids is a form of a Josephson coupling in quadratic order in terms of both the condensations. They further found

that the two condensates can coexist under weak magnetic fields, and the parameter region of the D_4 -BN phase is enhanced to the whole 3P_2 superfluid region. These results indicate that the internal structure of 3P_2 vortices and the thermodynamic properties of the coexistence phase are strongly influenced by the interplay between the two superfluid components. However, a full microscopic simulation of 3P_2 vortex dynamics in the coexistence phase has not yet been carried out.

In the outer core, the 3P_2 superfluid phase hosts vortices with qualitatively different properties from those in the inner crust, including the possibility of HQVs [59]. Building on this distinction, the authors in Ref. [82] proposed that the coupling between outer-core 3P_2 vortices and inner-crust 1S_0 vortices gives rise to a large-scale vortex network, which they identified as a candidate mechanism for pulsar glitches. They obtained a scaling law of the glitch energy that can explain the same law from the observation without any fine tuning parameters. Despite this proposal, a microscopic analysis of the structure and dynamics of 3P_2 vortices, as well as their interaction with proton superconducting flux tubes in the outer core, has not yet been carried out [83]. In particular, if the 3P_2 superfluid in the outer core and 1S_0 in the inner crust are overlapped in a certain region, vortices in these superfluids meet with forming junctions called boojums. These are key ingredients for a large-scale vortex network mentioned above. Josephson currents across the 3P_2 - 1S_0 boundary were also studied [84]. The time-dependent oscillating Josephson current induced by vortex motion produces electromagnetic radiation whose power far exceeds Ohmic dissipation, potentially contributing to neutron star heating during the photon cooling era. We mention here that noncoexistence of s-wave and p-wave pairing was discussed in ultracold atomic gases [85].

In this work, we investigate the microscopic interaction between 3P_2 and 1S_0 superfluid vortices in the mixture of 3P_2 and 1S_0 superfluids, by extending the thermodynamic analysis of Ref. [81] to include spatially inhomogeneous vortex configurations. We use the Gross-Pitaevskii (GP) equation valid at zero temperature with leaving coefficients of interactions free parameters, in contrast to the GL formalism valid near the transition temperature [86]. Building on the microscopic vortex structure identified in Ref. [51], we evaluate how the coupling between these two vortex species with the aim to provide a quantitative basis for understanding the diversity of observed glitch phenomena beyond the reach of the conventional avalanche model. We find a vortex molecule of a form of HQV-SQV-HQV, consisting of a single SQV in the 1S_0 condensate and two HQVs in the 3P_2 condensate each of which is connected by a domain wall to the SQV due to the quadratic Josephson coupling.

Such a vortex molecule structure is a salient signal in multi-component condensations in condensed matter systems. Two HQVs are connected by a domain wall in two-component Bose-Einstein condensates (BECs) [87–95], two-gap or two-component superconductors [96–99], and chiral p-wave superconductors [100,101]. Such configurations were extended to more complicated vortex molecules in multicomponent systems [102–107] and/or arbitrary charges [108,109].

This article is organized as follows. In Sec. II, we introduce the GP framework used to describe coexisting $^3\text{P}_2$ and $^1\text{S}_0$ superfluids, including $^3\text{P}_2$ and $^1\text{S}_0$ interaction and outline the numerical procedure for various vortex configurations. In Sec. IV, we present the results of GP calculations and discuss how vortex configurations change depending on the coupling constants for the interaction terms. Finally, a summary and prospect are given in Sec. V.

II. METHODS

A. Total free energy functional

We consider the phase boundary between the inner crust and the outer core of a neutron star, where $^1\text{S}_0$ and $^3\text{P}_2$ neutron superfluids may coexist. To describe such a coexisting phase of $^1\text{S}_0$ and $^3\text{P}_2$ neutron superfluids, we employ the GP equations. In this article, we denote the complex scalar order parameter of the $^1\text{S}_0$ superfluid as $\sigma(\mathbf{r})$, while the five-component complex spinor of the $^3\text{P}_2$ superfluid is denoted as $\vec{\psi}(\mathbf{r}) = (\psi_{-2}(\mathbf{r}), \psi_{-1}(\mathbf{r}), \psi_0(\mathbf{r}), \psi_1(\mathbf{r}), \psi_2(\mathbf{r}))$. We restrict our numerical analyses to two-dimensional (2D) coordinate space, while the equations will be given in a general form that can be applied to three-dimensional (3D) systems.

The total free energy functional of the mixed system of $^1\text{S}_0$ and $^3\text{P}_2$ superfluids is given by

$$F_{\text{total}}[\sigma, \vec{\psi}] = F_{\text{singlet}}[\sigma] + F_{\text{triplet}}[\vec{\psi}] + F_{\text{int}}[\sigma, \vec{\psi}], \quad (1)$$

where $F_{\text{singlet}}[\sigma]$ and $F_{\text{triplet}}[\vec{\psi}]$ are the free energy functionals of the $^1\text{S}_0$ and $^3\text{P}_2$ condensates, respectively, and $F_{\text{int}}[\sigma, \psi_m]$ accounts for the inter-condensate interaction. Each term is discussed in detail in the following subsections, Secs. II B, II C, and II D, respectively. The equilibrium configurations of $\sigma(\mathbf{r})$ and $\vec{\psi}(\mathbf{r})$ are obtained by minimizing F_{total} with respect to each order parameter, yielding the coupled Euler–Lagrange equations:

$$\frac{\delta F_{\text{total}}}{\delta \sigma^*} = 0, \quad (2)$$

$$\frac{\delta F_{\text{total}}}{\delta \psi_m^*} = 0 \quad (m = -2, \dots, 2). \quad (3)$$

In practice, these equations are solved numerically using the imaginary-time method, as described in Sec. III B.

B. GP for $^1\text{S}_0$ neutron superfluid

The $^1\text{S}_0$ neutron superfluid is characterized by a complex scalar order parameter $\sigma(\mathbf{r})$, which represents the condensate of spin-singlet Cooper pairs. Within the GP framework, the free energy functional is given by

$$F_{\text{singlet}}[\sigma] = \int d^3\mathbf{r} \left[\frac{\hbar^2}{2M} |\nabla\sigma|^2 + U_{\text{trap}}(\mathbf{r}) |\sigma|^2 + \frac{g_0}{2} |\sigma|^4 \right], \quad (4)$$

where $M = 2m_n$ is the mass of a neutron Cooper pair, and g_0 are constants that control the Landau potential. The first term is the gradient energy, which penalizes spatial variations of the order parameter and governs the coherence length of the condensate. The second term is the trapping potential needed to confine the condensates in a finite region.

C. GP for $^3\text{P}_2$ Neutron Cooper Pairs

Since the total angular momentum of a $^3\text{P}_2$ Cooper pair is $J = 2$, the $^3\text{P}_2$ neutron superfluid can be formally modeled as a spin-2 spinor Bose–Einstein condensate (BEC). We therefore adopt the spin-2 GP framework [110,111] to describe the $^3\text{P}_2$ condensate. Among possible phases of the spin-2 BECs, the relevant for the $^3\text{P}_2$ neutron superfluid is the nematic phase [112,113]. The total free energy functional of the $^3\text{P}_2$ superfluid reads [110]

$$F_{\text{triplet}}[\Psi] = \int d^3\mathbf{r} \left\{ \sum_{m=-2}^2 \psi_m^*(\mathbf{r}) \left[-\frac{\hbar^2}{2M} \nabla^2 + U_{\text{trap}}(\mathbf{r}) \right] \psi_m(\mathbf{r}) + \frac{c_0}{2} n^2(\mathbf{r}) + \frac{c_1}{2} |\mathbf{F}(\mathbf{r})|^2 + \frac{c_2}{2} |A_{00}(\mathbf{r})|^2 \right\}, \quad (5)$$

where $n(\mathbf{r})$ is the total superfluid density, $n(\mathbf{r}) = \sum_{m=-2}^2 |\psi_m(\mathbf{r})|^2$, $\mathbf{F}(\mathbf{r})$ is the spin-density vector, and $A_{00}(\mathbf{r})$ is a quantity that characterizes the spin-singlet Cooper pairs. c_i ($i = \{0, 1, 2\}$) are coupling constants that characterize the density-density, spin-spin, and spin-singlet pair interactions, respectively. The spin-density vector $\mathbf{F}(\mathbf{r})$ is defined by

$$F_v(\mathbf{r}) = \sum_{m,m'=-2}^2 \psi_m^*(\mathbf{r}) (f_v)_{mm'} \psi_{m'}(\mathbf{r}) \quad (v = x, y, z), \quad (6)$$

where $\mathbf{f} = (f_x, f_y, f_z)$ are the standard 5×5 spin matrices for spin-2, whose explicit forms can be found in, *e.g.*, Ref. [110]. $A_{00}(\mathbf{r})$ is given by [110]

$$A_{00}(\mathbf{r}) \equiv \frac{1}{\sqrt{5}} [2\psi_2(\mathbf{r})\psi_{-2}(\mathbf{r}) - 2\psi_1(\mathbf{r})\psi_{-1}(\mathbf{r}) + \psi_0^2(\mathbf{r})] = \frac{1}{\sqrt{5}} \text{tr}(A^2), \quad (7)$$

which is related to Ψ_{20} defined in Eq. (11) below by $A_{00} = \Psi_{20}/\sqrt{5}$.

The time-dependent GP equations are obtained by taking the functional derivative of F_{triplet} with respect to ψ_m^* :

$$i\hbar \frac{\partial \psi_m}{\partial t} = \frac{\delta F_{\text{total}}}{\delta \psi_m^*}, \quad (8)$$

yielding the coupled equations for each component m [110]. Equilibrium vortex configurations are obtained by evolving Eq. (8) in imaginary time ($t \rightarrow -i\tau$), as described in Sec. III B.

The $^3\text{P}_2$ superfluid order parameter is represented by a 3×3 complex symmetric matrix A_{ij} ($i, j = x, y, z$), which encodes

the spin-triplet, p -wave pairing structure of the condensate. Following Ref. [114], the matrix A_{ij} can be decomposed in terms of the magnetic quantum number components ψ_m ($m = -2, \dots, 2$) as

$$A_{ij} = \sum_{m=-2}^2 \psi_m \left(\mathcal{Y}_m^{(2)} \right)_{ij}, \quad (9)$$

where $\mathcal{Y}_m^{(2)}$ are the rank-2 symmetric traceless tensors constructed from the spin-2 spherical harmonics, forming a basis for the irreducible representation of the rotation group $\text{SO}(3)$ in the spin-2 sector [114].

A gauge-invariant scalar quantity characterizing the condensate can be constructed from the trace of A^2 . We define

$$\Psi_{20} \equiv \text{tr}(A^2) = \sum_{i,j} A_{ij} A_{ji}, \quad (10)$$

which is invariant under $\text{SO}(3)$ spin rotations but transforms nontrivially under the $\text{U}(1)$ gauge transformation $A_{ij} \rightarrow e^{2i\alpha} A_{ij}$, acquiring a phase $e^{4i\alpha}$. Substituting Eq. (9) into Eq. (10) and using the orthogonality of the basis tensors $\mathcal{Y}_m^{(2)}$, one obtains

$$\Psi_{20} = \text{tr}(A^2) = \sum_{m=-2}^2 (-1)^m \psi_m \psi_{-m}, \quad (11)$$

where the factor $(-1)^m$ arises from the contraction of the basis tensors, reflecting the time-reversal properties of the spin-2 representation [114].

The quantity Ψ_{20} plays a central role in identifying the positions of HQVs in the ${}^3\text{P}_2$ condensate. Under a 2π rotation around a HQV, the order parameter ψ_m acquires a phase $e^{i\pi} = -1$, leaving the physical state unchanged due to the discrete \mathbb{Z}_2 symmetry of the order parameter manifold [59]. Consequently, Ψ_{20} , being quadratic in ψ_m , acquires a phase of $e^{2i\pi} = 1$ under a single circuit around a HQV, whereas it winds by $e^{4i\pi}$ around an SQV. This distinction makes Ψ_{20} a sensitive probe of the vortex topology: the phase singularities of Ψ_{20} —points around which its phase winds by 2π —correspond to the cores of individual HQVs, as opposed to the integer vortices of σ . The vortex core positions of the HQVs are therefore identified numerically by locating the phase singularities of $\Psi_{20}(\mathbf{r})$ on the simulation lattice.

D. Interaction term

In the coexistence region near the boundary between the inner crust and the outer core, both the ${}^1\text{S}_0$ and ${}^3\text{P}_2$ superfluid phases are expected to be present simultaneously. In this region, the two order parameters ψ_m and σ are coupled through an interaction term in the free energy functional. Following the GL framework, and adopting the structure of the coupling term introduced in Ref. [81], the interaction free energy be-

tween the two superfluid components can be written as

$$\begin{aligned} F_{\text{int}}[\Psi, \sigma] &= \int d^3\mathbf{r} \left[\zeta_1 |\sigma|^2 \text{tr}(A^* A) + \zeta_2 (\sigma^2 \text{tr}(A^{*2}) + \sigma^{*2} \text{tr}(A^2)) \right] \\ &= \int d^3\mathbf{r} \sum_{m=-2}^2 \left[\zeta_1 |\sigma|^2 |\psi_m|^2 \right. \\ &\quad \left. + \zeta_2 \{ (-1)^m \sigma^2 \psi_m^{*2} + (-1)^m \sigma^{*2} \psi_m^2 \} \right], \quad (12) \end{aligned}$$

where ζ_1 and ζ_2 are real coupling constants defined as

$$\zeta_{1,2} = \tilde{\zeta}_{1,2} \frac{4\pi\hbar^2}{M}, \quad (13)$$

with parameters $\tilde{\zeta}_{1,2}$. This normalization is adopted so that $\zeta_{1,2}$ carry the same dimensions as the coupling constant g_0 in Eqs. (4) and (5), allowing for a direct comparison of the interaction strengths between the two condensates. The dimensionless values $\tilde{\zeta}_{1,2}$ are varied independently in the present numerical analysis.

The first term, proportional to ζ_1 , describes a density-density coupling between the two condensates, which is invariant under independent $\text{U}(1)$ phase rotations of each order parameter. The second term, proportional to ζ_2 , represents a coherent pair-exchange interaction between the two superfluid components, which breaks the relative $\text{U}(1)$ phase symmetry between ψ_m and σ . This type of coupling is analogous to the Rabi interaction known in coupled superconductors [81], and plays a crucial role in determining the structure and dynamics of quantized vortices near the phase boundary between the inner crust and the outer core. This coupling is analogous to the Rabi coupling in the context of BECs, in which it is linear with respect to both the condensates. In this work, we refer to this coupling as the Josephson term (Eq. (18)). The relative magnitude and sign of ζ_1 and ζ_2 control whether the interaction is attractive or repulsive between the two condensates, and are determined from microscopic considerations in the present analysis.

III. COMPUTATIONAL DETAILS

A. Trapping potential and discretization

Numerical simulations are performed on a two-dimensional square lattice, where all fields are discretized on a uniform mesh of grid points. To confine the condensate within a finite computational domain, we introduce a trapping potential $U_{\text{trap}}(\mathbf{r})$ defined as a function of the radial distance $r = |\mathbf{r}|$ from the center of the simulation box. The potential is characterized by a trap radius R_{trap} and a smoothing interval δ , and

is given by

$$U_{\text{trap}}(r) = \begin{cases} 0 & r < R_{\text{trap}} - \delta, \\ V \left(\frac{1}{2} - \frac{1}{2} \tanh \left[\pi \tan \left(\frac{\pi}{2\delta} (r - R_{\text{trap}}) \right) \right] \right)^{-1} & R_{\text{trap}} - \delta \leq r \leq R_{\text{trap}} + \delta, \\ V & r > R_{\text{trap}} + \delta, \end{cases} \quad (14)$$

where V is a large positive constant that effectively excludes the condensate from the region outside the trap. The intermediate region $R_{\text{trap}} - \delta \leq r \leq R_{\text{trap}} + \delta$ provides a smooth crossover between the flat interior and the hard wall, suppressing numerical artifacts arising from abrupt potential steps.

B. Vortex initialization and imaginary-time evolution

Quantized vortices are introduced by imprinting the desired phase winding onto each order parameter by hand. Specifically, a phase profile corresponding to the target vortex number is assigned to ψ_m and σ as initial conditions, and the system is then evolved in imaginary time to relax toward the energetically favored vortex configuration. This procedure yields the equilibrium spatial arrangement and number of vortices for a given set of parameters.

In the imaginary time evolution, we solve these equations:

$$\begin{aligned} -\hbar \frac{\partial \sigma}{\partial \tau} &= \left[-\frac{\hbar^2}{2M} \nabla^2 + U_{\text{trap}}(\mathbf{r}) + g_0 |\sigma|^2 \right] \sigma \\ &+ \sum_{m=-2}^2 [\zeta_1 |\psi_m|^2 \sigma + 2(-1)^m \zeta_2 \sigma^* \psi_m], \quad (15) \\ -\hbar \frac{\partial \psi_m}{\partial \tau} &= \left[-\frac{\hbar^2}{2M} \nabla^2 + U_{\text{trap}}(\mathbf{r}) + c_0 n(\mathbf{r}) \right] \psi_m \\ &+ \sum_{m'=-2}^2 c_1 \mathbf{F}^* \cdot (\mathbf{f})_{mm'} \psi_{m'} + c_2 \frac{1}{5} \psi_m^* \Psi_{20} \\ &+ \zeta_1 |\sigma|^2 \psi_m + 2(-1)^m \zeta_2 \psi_m^* \sigma^2, \quad (16) \end{aligned}$$

where τ represents the imaginary time.

At each step of the imaginary-time evolution, the order parameters are renormalized so that the integrated particle numbers of the 1S_0 and 3P_2 condensates are separately conserved. Specifically, after each update step, $\sigma(\mathbf{r})$ and $\psi_m(\mathbf{r})$ are rescaled such that

$$\int d^3\mathbf{r} |\sigma(\mathbf{r})|^2 = N, \quad \int d^3\mathbf{r} \sum_{m=-2}^2 |\psi_m(\mathbf{r})|^2 = N, \quad (17)$$

where the particle number N is held fixed and equal for both condensates throughout the evolution. This normalization condition ensures that the imaginary-time evolution converges to the ground state at fixed particle number for each component, rather than allowing the condensate densities to drift freely.

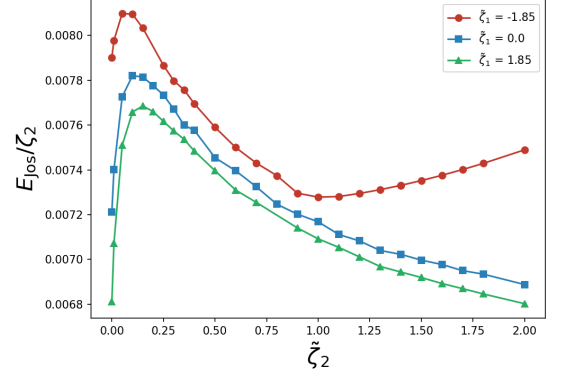


FIG. 1: Josephson term density $\int d^3\mathbf{r} \sum_{m=-2}^2 [(-1)^m \sigma^2 \psi_m^{*2} + (-1)^m \sigma^* \psi_m^2]$ as a function of the pair-exchange coupling constant ζ_2 for three values of the density-density coupling constant ζ_1 , as indicated in the legend. The system consists of one SQV in the 1S_0 condensate and two HQVs in the 3P_2 condensate.

C. Vortex pinning and activation of the interaction term

To analyze the dynamics triggered by the 1S_0 - 3P_2 coupling, we adopt the following two-stage protocol. In the first stage, the coupling constants are set to $\zeta_1 = \zeta_2 = 0$, decoupling the two superfluid components entirely. In this decoupled state, artificial pinning potentials are introduced for both the singlet and triplet order parameters independently. Each pinning site is modeled as a repulsive potential with a small spatial extent, and vortices are pinned at prescribed locations by hand.

In the second stage, the interaction terms ζ_1 and ζ_2 are activated, restoring the coupling between the 1S_0 and 3P_2 condensates. The subsequent real-time evolution of the system is then analyzed to examine how the inter-condensate interaction drives vortex depinning and governs the ensuing vortex dynamics. This protocol allows us to isolate the role of the coupling terms in the glitch-like phenomena observed in the simulation.

IV. RESULTS AND DISCUSSION

A. Vortex Shapes and Vortex Interaction

To further characterize the nature of the inter-condensate coupling, we introduce the *Josephson energy*, defined as the contribution to the interaction free energy arising from the relative phase between the 1S_0 and 3P_2 condensates. Extracting the phase-sensitive part of Eq. (12), the Josephson energy density is given by

$$\mathcal{E}_{\text{Jos}}(\mathbf{r}) = \zeta_2 \sum_{m=-2}^2 [(-1)^m \sigma^2 \psi_m^{*2} + (-1)^m \sigma^* \psi_m^2], \quad (18)$$

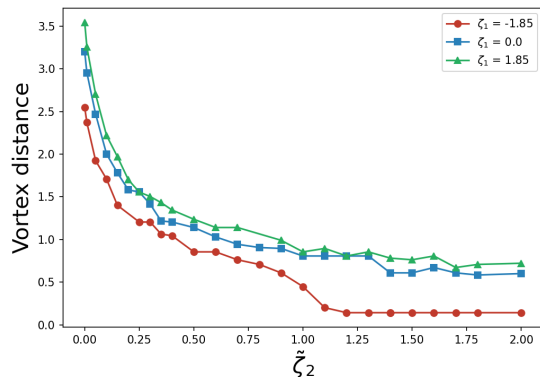


FIG. 2: Inter-vortex distance d_{HQV} between the two HQVs in the ${}^3\text{P}_2$ condensate as a function of the pair-exchange coupling constant ζ_2 for three values of the density–density coupling constant ζ_1 , as indicated in the legend. The HQV positions are identified from the phase singularities of $\Psi_{20}(\mathbf{r})$ as described in Sec. II C. The system configuration and imaginary-time evolution procedure are the same as in Fig. 1.

and the total Josephson energy is obtained by integrating over the simulation domain,

$$E_{\text{Jos}} = \int d^3\mathbf{r} \mathcal{E}_{\text{Jos}}(\mathbf{r}). \quad (19)$$

The spatial distribution of $\mathcal{E}_{\text{Jos}}(\mathbf{r})$ is shown in Fig. 1. A pronounced variation of the Josephson energy is observed in the vicinity of the vortex cores, where the phase fields θ_σ and θ_m wind rapidly. This spatial structure reflects the locking and unlocking of the relative phase between the two condensates as the vortices approach and interact with each other. In particular, the sign change of \mathcal{E}_{Jos} across the vortex core indicates a local reversal of the effective Josephson coupling, which we identify as a key driver of the inter-vortex force between the ${}^1\text{S}_0$ and ${}^3\text{P}_2$ vortices.

To investigate the role of the pair-exchange coupling on the inter-vortex interaction, we compare the Josephson energy for a system consisting of one SQV in the ${}^1\text{S}_0$ condensate and two HQVs in the ${}^3\text{P}_2$ condensate, where the total vorticity of the two HQVs equals that of the SQV. This configuration is motivated by the vortex network model of Ref. [82], in which ${}^1\text{S}_0$ and ${}^3\text{P}_2$ vortices are connected across the phase boundary.

Figure 1 shows the spatial distribution of the Josephson energy density $\mathcal{E}_{\text{Jos}}(\mathbf{r})$, normalized by ζ_2 , for several values of the coupling constant ζ_2 . Since \mathcal{E}_{Jos} is linear in ζ_2 by construction [see Eq. (18)], plotting $\mathcal{E}_{\text{Jos}}/\zeta_2$ isolates the geometric contribution arising purely from the phase structure of the vortices, independently of the coupling strength.

The normalized Josephson energy distribution reflects the relative phase field $\Delta\theta_m = \theta_\sigma - \theta_m$ between the SQV and each HQV. As ζ_2 is varied, the total Josephson energy E_{Jos} scales linearly, while the spatial profile of $\mathcal{E}_{\text{Jos}}/\zeta_2$ remains unchanged, confirming that the geometric structure of the phase winding governs the distribution of the Josephson energy independently of ζ_2 . This result demonstrates that the pair-exchange coupling ζ_2 acts as a tunable parameter controlling

the effective Josephson-like force between the ${}^1\text{S}_0$ SQV and the ${}^3\text{P}_2$ HQVs, with direct implications for the vortex depinning dynamics relevant to the glitch mechanism.

To quantify the spatial separation between the two HQVs in the ${}^3\text{P}_2$ condensate, we extract the positions of the phase singularities of the order parameter component $\psi_{20}(\mathbf{r})$. A phase singularity is defined as a point around which the phase of ψ_{20} winds by 2π , corresponding to the core of a quantized vortex. Numerically, the singularity positions are identified by evaluating the phase winding number

$$n = \frac{1}{2\pi} \oint_{\mathcal{C}} \nabla\theta_{20}(\mathbf{r}) \cdot d\mathbf{l} \quad (20)$$

along closed contours \mathcal{C} encircling each candidate point on the simulation lattice, where $\theta_{20}(\mathbf{r}) = \arg[\psi_{20}(\mathbf{r})]$ is the local phase of ψ_{20} . A site is identified as a vortex core when $n = \pm 1$.

Figure 2 shows the inter-vortex distance d_{HQV} as a function of ζ_2 for several values of ζ_1 . The results demonstrate that d_{HQV} decreases monotonically with increasing ζ_2 , regardless of the value or sign of ζ_1 . The total Josephson energy E_{Jos} as a function of ζ_2 is shown in Fig. 1, where E_{Jos} is found to decrease with increasing ζ_2 , consistent with the attractive nature of the pair-exchange interaction driving the HQVs toward the SQV. To investigate the origin and implications of this behavior, we analyze the spatial configurations of the ${}^1\text{S}_0$ and ${}^3\text{P}_2$ vortices and the distribution of the Josephson energy density [Eq. (18)] for $\zeta_1 = 0$ and three representative values of ζ_2 . The results are shown in Figs. 3, 4, and 5.

Figure 2 also indicates that the sign of ζ_1 affects the vortex distance. The positive (negative) ζ_1 increases (decreases) the distance compared with the case of $\zeta_1 = 0$. This implies that positive (negative) ζ_1 yields repulsion (attraction) between the vortices. This is consistent with the case of two-component BECs [115]. In particular, when ζ_1 is attractive, the inter-vortex attraction becomes more pronounced at shorter vortex separations, and the two HQVs ultimately merge into a single vortex as the HQV–HQV distance vanishes.

When ζ_2 is very small, the inter-vortex distance d_{HQV} is large, and the total Josephson energy E_{Jos} takes a correspondingly large value, as shown in Fig. 1. As ζ_2 is increased, d_{HQV} decreases rapidly (Fig. 2), accompanied by a reduction in E_{Jos} (Fig. 1). These results indicate that the pair-exchange coupling ζ_2 induces a strong attractive interaction between the HQVs and the SQV, and that this attraction is driven by the minimization of the Josephson energy.

This interpretation is further supported by the spatial distributions shown in Figs. 3, 4, and 5. As ζ_2 increases, the Josephson energy density [Eq. (18)], which reflects the relative phase between the ${}^1\text{S}_0$ and ${}^3\text{P}_2$ condensates, tends to align toward a uniform sign throughout the simulation domain. This alignment indicates that a configuration in which the two HQVs and one SQV are co-located is energetically more favorable than one in which the HQVs are spatially separated from the SQV, since the former minimizes the total Josephson energy. As a result, the two HQVs and the SQV interact attractively, and the system evolves toward a bound vortex configuration with increasing ζ_2 .

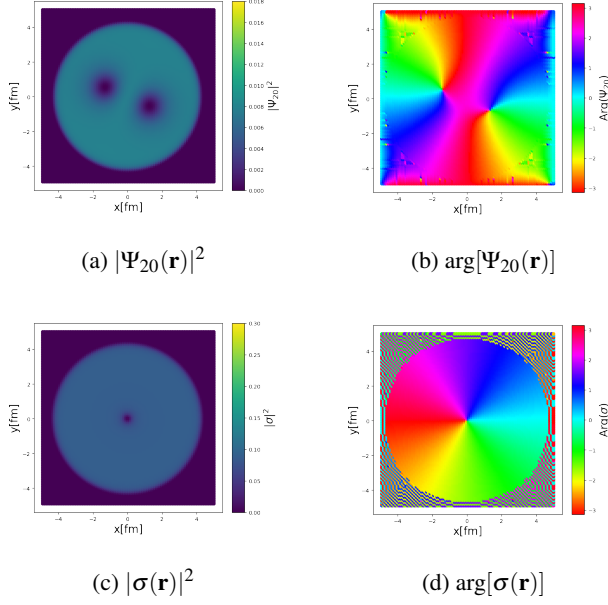


FIG. 3: Color maps of the ground-state configuration obtained by imaginary-time evolution without pinning potentials for both condensates and $\zeta_1 = 0, \zeta_2 = 0.010$ (a) Density $|\Psi_{20}|^2$ of the 3P_2 condensate, showing the two HQV cores as density-depleted regions. (b) Phase $\arg[\Psi_{20}]$ of the 3P_2 condensate, displaying the 2π phase winding around each HQV core. (c) Density $|\sigma|^2$ of the 1S_0 condensate, showing the SQV core as a single density-depleted region. (d) Phase $\arg[\sigma]$ of the 1S_0 condensate, displaying the 2π phase winding around the SQV core. (e) Spatial distribution of the Josephson energy density $\sigma^2 \text{tr}(A^{*2}) + \sigma^{*2} \text{tr}(A^2)$, reflecting the relative phase between the two condensates. All panels share the same spatial coordinates (x, y) .

B. Pinning distance and Josephson energy

To independently control the positions of the 1S_0 SQV and the 3P_2 HQVs, we introduce pinning potentials for each con-

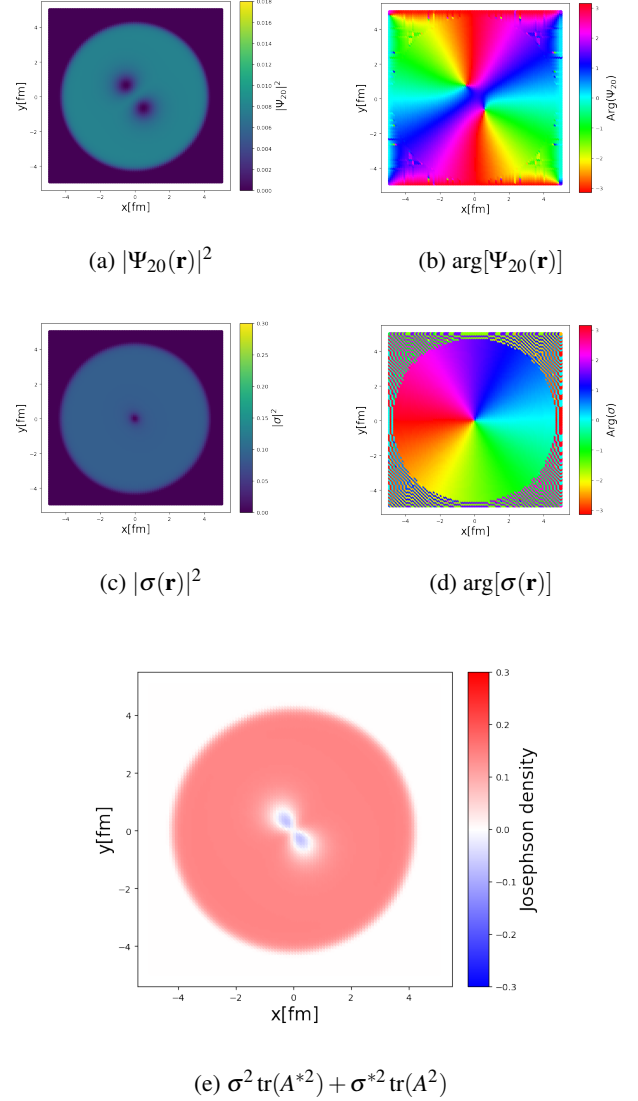


FIG. 4: Color maps of the ground-state configuration obtained by imaginary-time evolution without pinning potentials for both condensates and $\zeta_1 = 0, \zeta_2 = 0.150$. (a) Density $|\Psi_{20}|^2$ of the 3P_2 condensate, showing the two HQV cores as density-depleted regions. (b) Phase $\arg[\Psi_{20}]$ of the 3P_2 condensate, displaying the 2π phase winding around each HQV core. (c) Density $|\sigma|^2$ of the 1S_0 condensate, showing the SQV core as a single density-depleted region. (d) Phase $\arg[\sigma]$ of the 1S_0 condensate, displaying the 2π phase winding around the SQV core. (e) Spatial distribution of the Josephson energy density $\sigma^2 \text{tr}(A^{*2}) + \sigma^{*2} \text{tr}(A^2)$, reflecting the relative phase between the two condensates. All panels share the same spatial coordinates (x, y) .

densate separately. A pinning potential is introduced for the 1S_0 condensate as

$$F_{\text{pin}}^{(1S_0)} = \int d^3\mathbf{r} V_{\text{trap}}(\mathbf{r}) |\sigma(\mathbf{r})|^2, \quad (21)$$

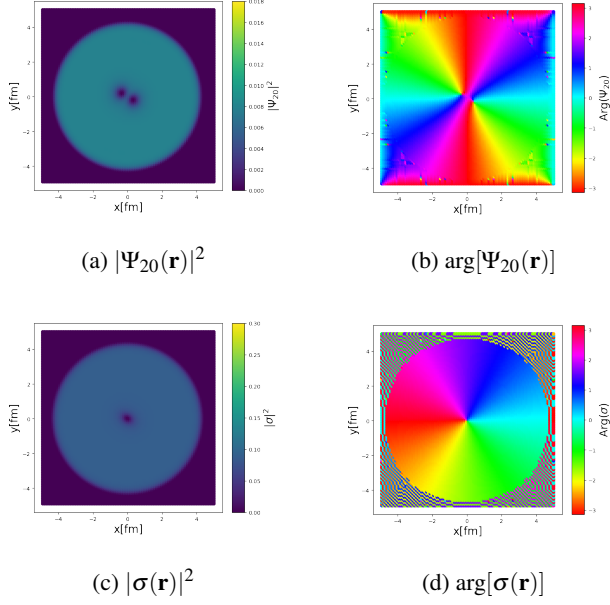


FIG. 5: Color maps of the ground-state configuration obtained by imaginary-time evolution without pinning potentials for both condensates and $\zeta_1 = 0$, $\zeta_2 = 1.000$. (a) Density $|\Psi_{20}|^2$ of the 3P_2 condensate, showing the two HQV cores as density-depleted regions. (b) Phase $\arg[\Psi_{20}]$ of the 3P_2 condensate, displaying the 2π phase winding around each HQV core. (c) Density $|\sigma|^2$ of the 1S_0 condensate, showing the SQV core as a single density-depleted region. (d) Phase $\arg[\sigma]$ of the 1S_0 condensate, displaying the 2π phase winding around the SQV core. (e) Spatial distribution of the Josephson energy density $\sigma^2 \text{tr}(A^{*2}) + \sigma^{*2} \text{tr}(A^2)$, reflecting the relative phase between the two condensates. All panels share the same spatial coordinates (x, y) .

which pins the SQV core of the 1S_0 condensate at a separate location. For the 3P_2 condensate, a pinning potential is coupled to the gauge-invariant density $|\Psi_{20}(\mathbf{r})|^2$, adding the

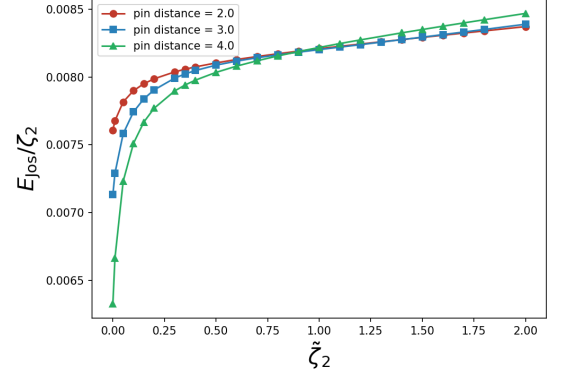


FIG. 6: Josephson term density $\int d^3\mathbf{r} \sum_{m=-2}^2 [(-1)^m \sigma^2 \psi_m^{*2} + (-1)^m \sigma^{*2} \psi_m^2]$ as a function of the pair-exchange coupling constant ζ_2 for three values of the pinning site distances of HQV, as indicated in the legend. Here, $\zeta_1 = 0$. The system consists of one SQV in the 1S_0 condensate and two HQVs in the 3P_2 condensate, with singlet and triplet pinning position.

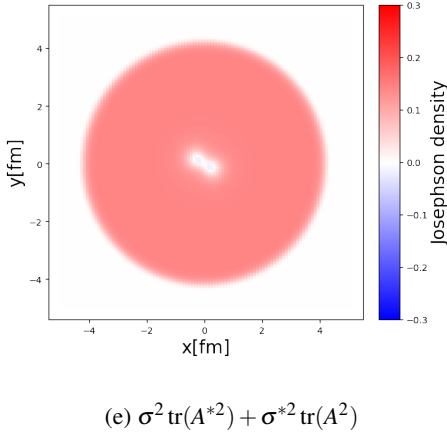


FIG. 7: Inter-vortex distance d_{HQV} between the two HQVs in the 3P_2 condensate as a function of the pair-exchange coupling constant ζ_2 for three values of the pinning site of HQV, as indicated in the legend. The HQV positions are identified from the phase singularities of $\Psi_{20}(\mathbf{r})$ as described in Sec. II C. The system configuration and imaginary-time evolution procedure are the same as in Fig. 6.

following term to the free energy functional:

$$F_{\text{pin}}^{(3P_2)} = \int d^3\mathbf{r} V_{\text{trap}}(\mathbf{r}) |\Psi_{20}(\mathbf{r})|^2, \quad (22)$$

where $V_{\text{trap}}(\mathbf{r})$ is a spatially localized repulsive potential centered at the desired vortex position. Since $\Psi_{20} = \text{tr}(A^2) = \sum_m (-1)^m \psi_m \psi_{-m}$ vanishes at the core of each HQV [see Eq. (11)], this term energetically favors the suppression of $|\Psi_{20}|^2$ at the potential center, thereby pinning the HQV cores at prescribed locations.

The full protocol proceeds as follows. In the first stage, the inter-condensate coupling is switched off ($\zeta_1 = \zeta_2 = 0$), and both the condensates are evolved independently in the imagi-

nary time with the pinning potentials active. This yields a configuration in which one SQV of the 1S_0 condensate and two HQVs of the 3P_2 condensate are pinned at spatially separated, prescribed positions. In the second stage, the pair-exchange coupling ζ_2 is activated and the system is again evolved in the imaginary time to a new energy minimum, while the pinning potentials remain in place.

To systematically characterize the effect of the inter-condensate interaction, this procedure is repeated for several values of ζ_2 , with ζ_1 held fixed $\zeta_1 = 0$. For each value of ζ_2 , we record (i) the total Josephson energy E_{Jos} defined in Eq. (18), and (ii) the spatial configuration and morphology of the vortex cores, as determined from the phase singularities of $\sigma(\mathbf{r})$ and $\Psi_{20}(\mathbf{r})$ following the procedure described in Sec. II. The results are presented in Figs. 6 and 7, which show, respectively, the ζ_2 -dependence of the normalized Josephson energy density and the inter-HQV distance as a function of ζ_2 .

To directly measure the attractive force between the HQVs and the SQV, we introduce pinning sites and trap the 3P_2 HQVs and the 1S_0 SQV at spatially separated locations, as described in Sec. III C. As shown in Fig. 7, when ζ_2 is increased beyond a critical value, the HQVs are no longer confined to their pinning sites and are instead attracted toward the SQV. The resulting inter-vortex distance closely coincides with that obtained in the absence of pinning potentials (Fig. 2), confirming that the Josephson-energy-driven attraction dominates over the pinning force for sufficiently large ζ_2 .

The critical value of ζ_2 at which depinning occurs depends on the initial separation between the pinning sites: as shown in Fig. 7, the vortices pinned at closer separations require a larger ζ_2 to depin, indicating that the effective attractive force is weaker at shorter inter-vortex distances.

The spatial configurations of the vortices and the corresponding Josephson energy density distributions are shown in Figs. 8 and 9. In the weak-coupling regime, where ζ_2 is small and the vortices remain pinned, the domain wall of the Josephson energy density—the line along which the relative phase between the 1S_0 and 3P_2 condensates changes sign—is arranged so as to minimize the total Josephson energy (Fig. 8e). In addition, a pronounced distortion of the 3P_2 phase field is observed in this regime, reflecting the competition between the pinning potential and the inter-condensate coupling. In contrast, when ζ_2 is sufficiently large, depinning occurs and the 3P_2 HQVs leave their pinning sites and bind to the 1S_0 SQV, forming a composite vortex structure (Fig. 9).

V. SUMMARY AND PROSPECT

In this work, we have investigated the microscopic interaction between half-quantized vortices (HQVs) in the 3P_2 neutron superfluid and a singly-quantized vortex (SQV) in the 1S_0 neutron superfluid within a two-dimensional coexistence phase, using numerical simulations based on the Gross-Pitaevskii (GP) framework. We have demonstrated that the pair-exchange coupling ζ_2 , which gives rise to the Josephson energy term [Eq. (18)], induces a significant attractive interaction between the two 3P_2 HQVs and one 1S_0 SQV.

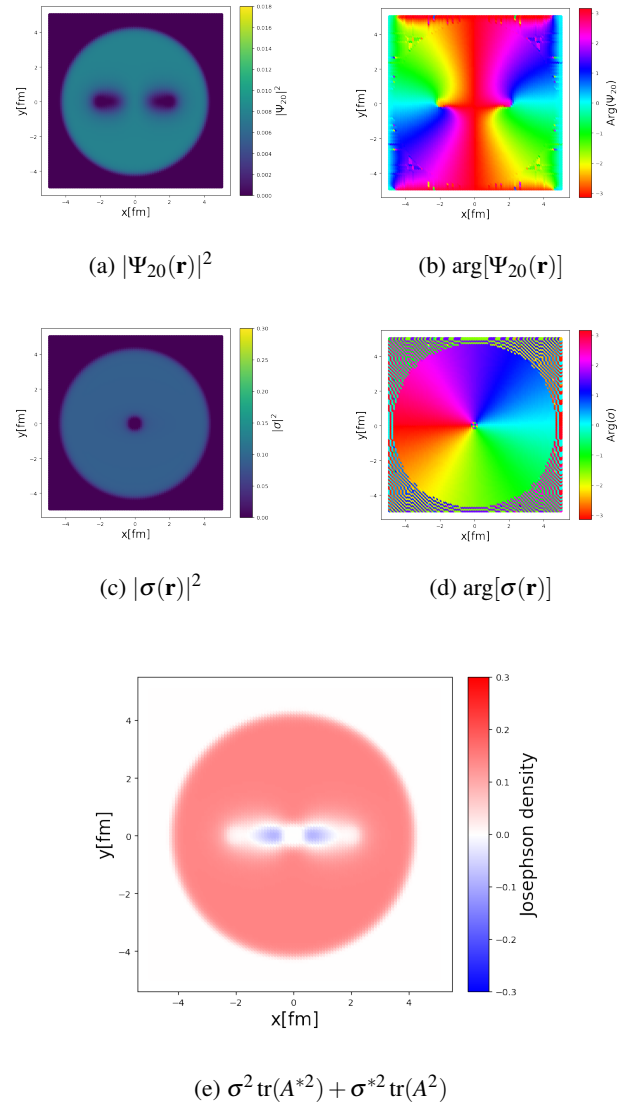


FIG. 8: Color maps of the ground-state configuration obtained by imaginary-time evolution with pinning potentials for both condensates and $\zeta_1 = 0$, $\zeta_2 = 0.150$. pin site is $(5.0, 5.0)$ for singlet SQV and $(5.0 \pm 2.0, 5.0)$ or triplet HQV. HQV distance is about 4.0 fm. (a) Density $|\Psi_{20}|^2$ of the 3P_2 condensate, showing the two HQV cores as density-depleted regions. (b) Phase $\arg[\Psi_{20}]$ of the 3P_2 condensate, displaying the 2π phase winding around each HQV core. (c) Density $|\sigma|^2$ of the 1S_0 condensate, showing the SQV core as a single density-depleted region. (d) Phase $\arg[\sigma]$ of the 1S_0 condensate, displaying the 2π phase winding around the SQV core. (e) Spatial distribution of the Josephson energy density $\sigma^2 \text{tr}(A^{*2}) + \sigma^{*2} \text{tr}(A^2)$, reflecting the relative phase between the two condensates. All panels share the same spatial coordinates (x, y) . Here, 2 HQVs are still pinned at pinning site.

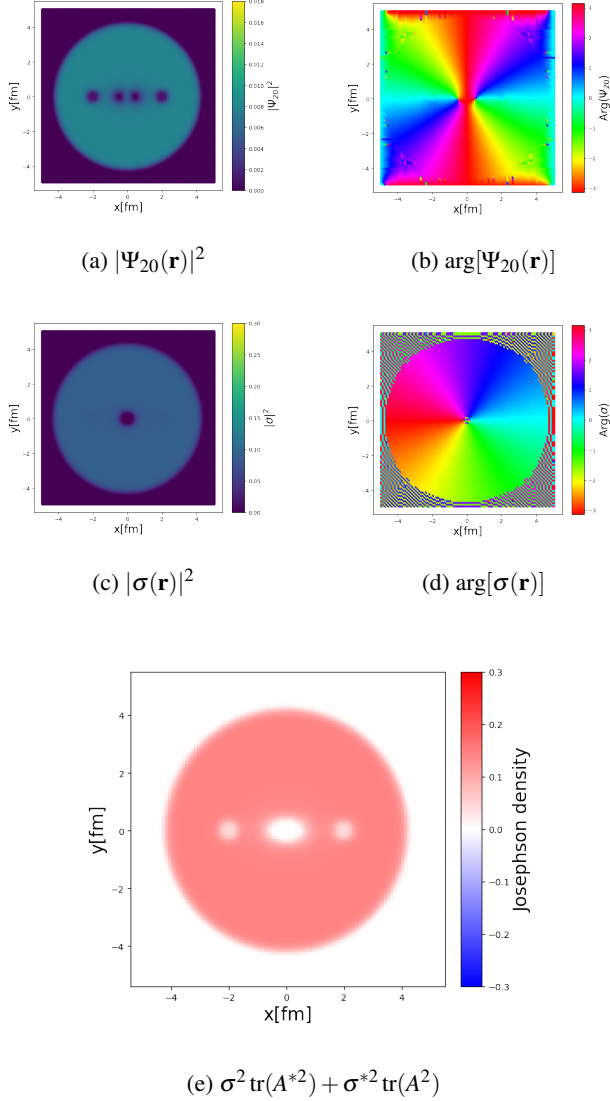


FIG. 9: Color maps of the ground-state configuration obtained by imaginary-time evolution with pinning potentials for both condensates and $\zeta_1 = 0$, $\zeta_2 = 1.000$. pin site is $(5.0, 5.0)$ for singlet SQV and $(5.0 \pm 2.0, 5.0)$ or triplet HQV. triplet pinning site distance is about 4.0 fm. (a) Density $|\Psi_{20}|^2$ of the 3P_2 condensate, showing the two HQV cores as density-depleted regions. (b) Phase $\arg[\Psi_{20}]$ of the 3P_2 condensate, displaying the 2π phase winding around each HQV core. (c) Density $|\sigma|^2$ of the 1S_0 condensate, showing the SQV core as a single density-depleted region. (d) Phase $\arg[\sigma]$ of the 1S_0 condensate, displaying the 2π phase winding around the SQV core. (e) Spatial distribution of the Josephson energy density $\sigma^2 \text{tr}(A^{*2}) + \sigma^{*2} \text{tr}(A^2)$, reflecting the relative phase between the two condensates. All panels share the same spatial coordinates (x, y) . Here, 2 HQVs are already unpinned and almost connect to the singlet vortex.

This attraction is strong enough to overcome the pinning potential applied to the 3P_2 vortices, driving them away from their pinning sites and toward the SQV. The resulting HQV–SQV–HQV bound configuration substantially alters the spatial arrangement of the 3P_2 vortices, providing microscopic evidence that the boojum structure proposed in Ref. [82] can indeed form at the phase boundary between the inner crust and the outer core of a neutron star. Furthermore, the strong attraction exerted on the 1S_0 SQV by the 3P_2 HQVs suggests that, if the triplet vortices are pinned by some mechanism, the singlet vortex will also experience an attractive force from the triplet vortices, potentially suppressing the relative motion of the two vortex species and affecting the dynamics relevant to the glitch mechanism.

We note that the present study constitutes a first step toward evaluating the role of the boojum structure in the vortex network model of Ref. [82] microscopically. The simulations are performed in two spatial dimensions under the assumption of a coexistence phase, which requires the phase boundary to be planar. A fully three-dimensional treatment will be needed to capture the realistic geometry of the inner-crust–outer-core boundary.

The present results motivate several directions for future work. First, three-dimensional simulations will allow us to evaluate how the HQV bends in the vicinity of a boojum, and whether the HQV–SQV connection can form a large-scale vortex network of the kind envisioned in Ref. [82]. Three-dimensional calculations are already underway. It is also important to investigate the effects of the Josephson coupling on vortex lattices, as studied in two-component BEC systems, since the collective behavior of coupled vortex lattices—in particular, whether the 1S_0 and 3P_2 vortex lattices lock together or slide independently—is directly relevant to the angular momentum transfer mechanism underlying the glitch phenomenon [90]. Second, the effect of the HQV–SQV attraction on the dynamics of the SQV itself will be assessed, as the suppression of SQV motion by pinned triplet vortices may have direct implications for the avalanche model of pulsar glitches. These microscopic results on the vortex–vortex coupling will then be used to evaluate the influence of the HQV–SQV attraction on the vortex network model and the avalanche mechanism, with the aim of providing a quantitative microscopic basis for the glitch mechanism. Additionally, the formation of a stable HQV–SQV–HQV molecular bound state opens the possibility of a novel oscillation mode arising from the attractive inter-vortex interaction. Such an inter-vortex vibrational mode could serve as a new internal heat source in neutron stars, with potential implications for neutron star cooling. The possibility of recombination and exchange of the HQV–SQV–HQV pair upon vortex collisions will also be examined in future work. For instance, exchanging a partner in a collision of two vortex molecules found in a two-component Bose-Einstein condensation (BEC) [94] may occur.

The significant role of the Josephson term found in this work suggests broader implications beyond neutron star physics. In finite nuclei, both spin-singlet and spin-triplet pairings are in principle possible, and recent studies have shown that spin-triplet pairing condensates can coexist with

spin-singlet pairing in even-even singly closed nuclei such as Ca and Sn isotopes [116]. The present results indicate that the Josephson coupling between singlet and triplet condensates—driven by their relative phase—can generate a strong inter-condensate interaction, suggesting that analogous Josephson effects may play an important role in finite nuclei where both 3P_2 and 1S_0 pairings coexist, as well as in proton–neutron systems coupled via the 3S_1 channel. To quantify these effects in realistic nuclear systems, it will be necessary to determine the triplet pairing coupling constant and the singlet–triplet interaction coefficient from experimental data on heavy nuclei such as Pb isotopes.

Furthermore, recent microscopic calculations based on superfluid band theory have indicated the emergence of spin-triplet pairing in the rod (pasta) phase of the neutron star inner crust, where two-dimensional crystalline structures, spin-orbit interactions, and strong magnetic fields act in concert [117]. Since the pasta phase is expected to occupy the high-density region of the inner crust near the crust–core boundary, the vortex dynamics in the vicinity of the pasta phase may be significantly influenced by the inter-condensate Josephson coupling identified in the present work, with potential implications for the glitch mechanism in this transitional region.

Finally, the inter-condensate interaction studied here is directly analogous to the Josephson coupling in two-component

BEC systems, as recently realized experimentally in bilayer superfluid systems [118,119]. The present framework is therefore also relevant to the broader context of multi-component condensate physics, including the dynamics of coupled half-integer and integer vortices in spinor BEC systems [51,110].

ACKNOWLEDGMENTS

This work is supported by JSPS Grant-in-Aid for Scientific Research KAKENHI Grants No. JP23K03410 (K. S.) and No. JP23K25864 (K. S.), No. JP25H01269 (K. S.) and JP23K22492 (M. N.). This work is also supported by JST SPRING, Grant Number JPMJSP JPMJSP2180 (T. H.) and by the Science Tokyo Support Program for Doctoral Students (T. H.), funded by the Universities for International Research Excellence. The work is also supported in part by the WPI program “Sustainability with Knotted Chiral Meta Matter (WPI-SKCM²)” at Hiroshima University (M. N.). This work used computational resources of the Yukawa–21 and Heian supercomputer at Yukawa Institute for Theoretical Physics (YITP), Kyoto University.

-
- [1] J. M. Lattimer and M. Prakash, *Physics Reports* **621**, 127 (2016), memorial Volume in Honor of Gerald E. Brown.
 - [2] B. Haskell and A. Sedrakian, Superfluidity and superconductivity in neutron stars, in *The Physics and Astrophysics of Neutron Stars*, edited by L. Rezzolla, P. Pizzochero, D. I. Jones, N. Rea, and I. Vidaña (Springer International Publishing, Cham, 2018) pp. 401–454.
 - [3] F. Özel and P. Freire, *Annual Review of Astronomy and Astrophysics* **54**, 401 (2016).
 - [4] M. C. Miller, F. K. Lamb, A. J. Dittmann, S. Bogdanov, Z. Arzumanian, K. C. Gendreau, S. Guillot, W. C. G. Ho, J. M. Lattimer, M. Loewenstein, S. M. Morsink, P. S. Ray, M. T. Wolff, C. L. Baker, T. Cazeau, S. Manthripragada, C. B. Markwardt, T. Okajima, S. Pollard, I. Cognard, H. T. Cromartie, E. Fonseca, L. Guillemot, M. Kerr, A. Parthasarathy, T. T. Pennucci, S. Ransom, and I. Stairs, *The Astrophysical Journal Letters* **918**, L28 (2021).
 - [5] T. E. Riley, A. L. Watts, P. S. Ray, S. Bogdanov, S. Guillot, S. M. Morsink, A. V. Bilous, Z. Arzumanian, D. Choudhury, J. S. Deneva, K. C. Gendreau, A. K. Harding, W. C. G. Ho, J. M. Lattimer, M. Loewenstein, R. M. Ludlam, C. B. Markwardt, T. Okajima, C. Prescod-Weinstein, R. A. Remillard, M. T. Wolff, E. Fonseca, H. T. Cromartie, M. Kerr, T. T. Pennucci, A. Parthasarathy, S. Ransom, I. Stairs, L. Guillemot, and I. Cognard, *The Astrophysical Journal Letters* **918**, L27 (2021).
 - [6] D. Page, M. Prakash, J. M. Lattimer, and A. W. Steiner, *Phys. Rev. Lett.* **106**, 081101 (2011).
 - [7] P. S. Shternin, D. G. Yakovlev, C. O. Heinke, W. C. G. Ho, and D. J. Patnaude, *Monthly Notices of the Royal Astronomical Society: Letters* **412**, L108 (2011).
 - [8] V. Graber, N. Andersson, and M. Hogg, *Int. J. Mod. Phys. D* **26**, 1730015 (2017), arXiv:1610.06882 [astro-ph.HE].
 - [9] A. Sedrakian and J. W. Clark, *Eur. Phys. J. A* **55**, 167 (2019), arXiv:1802.00017 [nucl-th].
 - [10] A. Sedrakian and P. B. Rau, *Spin effects in superfluidity, neutron matter and neutron stars* (2026), arXiv:2604.02782 [astro-ph.HE].
 - [11] J. A. S. M. A. Alpar, S. A. Langer, *Astrophys. J.* **282**, 533 (1984).
 - [12] M. Fujiwara, K. Hamaguchi, N. Nagata, and M. E. Ramirez-Quezada, *Journal of Cosmology and Astroparticle Physics* **2024** (03), 051.
 - [13] Y. B. Nam and K. Sekizawa, arXiv preprint (2025), arXiv:2510.24167.
 - [14] D. H. Staelin and E. C. Reifenstein, *Science* **162**, 1481 (1968), <https://www.science.org/doi/pdf/10.1126/science.162.3861.1481>.
 - [15] L. M., V. A., and M. B., *Nature* **220**, 340 (1968), <https://www.nature.com/articles/220340a0>.
 - [16] D. Antonopoulou, B. Haskell, and C. M. Espinoza, *Rept. Prog. Phys.* **85**, 126901 (2022).
 - [17] S. Zhou, E. Gügercinoğlu, J. Yuan, M. Ge, and C. Yu, *Universe* **8**, 641 (2022), arXiv:2211.13885 [astro-ph.HE].
 - [18] P. W. Anderson and N. Itoh, *Nature* **256**, 25 (1975).
 - [19] K. S. Cheng, D. Pines, M. A. Alpar, and J. Shaham, *ApJ* **330**, 835 (1988).
 - [20] L. Warszawski and A. Melatos, *MNRAS* **415**, 1611 (2011).
 - [21] Y. Mochizuki and T. Izuyama, *Astrophys. J.* **440**, 263 (1995).
 - [22] Y. S. Mochizuki, K. Oyamatsu, and T. Izuyama, *The Astrophysical Journal* **489**, 848 (1997).
 - [23] Y. Mochizuki, T. Izuyama, and I. Tanihata, *The Astrophysical Journal* **521**, 281 (1999).

- [24] P. Haensel, A. Potekhin, and D. Yakovlev, *Neutron Stars I: Equation of State and Structure*, Astrophysics and Space Science Library (Springer New York, 2007).
- [25] N. Andersson, K. Glampedakis, W. C. G. Ho, and C. M. Espinoza, *Phys. Rev. Lett.* **109**, 241103 (2012).
- [26] N. Chamel, *Phys. Rev. Lett.* **110**, 011101 (2013).
- [27] L. Warszawski and A. Melatos, *Mon. Not. R. Astrn. Soc.* **428**, 1911 (2012).
- [28] J. Piekarewicz, F. J. Fattoyev, and C. J. Horowitz, *Phys. Rev. C* **90**, 015803 (2014).
- [29] M. Antonelli, A. Montoli, and P. M. Pizzochero, Insights into the physics of neutron star interiors from pulsar glitches, in *Astrophysics in the XXI Century with Compact Stars* (WORLD SCIENTIFIC, 2022) Chap. Chapter 7, pp. 219–281.
- [30] P. S. Ray, S. Guillot, W. C. G. Ho, M. Kerr, T. Enoto, K. C. Gendreau, Z. Arzumanyan, D. Altamirano, S. Bogdanov, R. Campion, D. Chakrabarty, J. S. Deneva, G. K. Jaisawal, R. Kozon, C. Malacaria, T. E. Strohmayer, and M. T. Wolff, *The Astrophysical Journal* **879**, 130 (2019).
- [31] R. Dib, V. M. Kaspi, and F. P. Gavriil, *The Astrophysical Journal* **673**, 1044 (2008).
- [32] L. Amundsen and E. Ostgaard, *Nucl. Phys.* **A442**, 163 (1985).
- [33] T. Takatsuka and R. Tamagaki, *Prog. Theor. Phys. Suppl.* **112**, 27 (1993).
- [34] J. A. Sauls, Superfluidity in the interiors of neutron stars, in *Timing Neutron Stars*, edited by H. Ögelman and E. P. J. van den Heuvel (Springer Netherlands, Dordrecht, 1989) pp. 457–490.
- [35] M. Baldo, J. Cugnon, A. Lejeune, and U. Lombardo, *Nucl. Phys.* **A536**, 349 (1992).
- [36] O. Elgaroy, L. Engvik, M. Hjorth-Jensen, and E. Osnes, *Nucl. Phys.* **A607**, 425 (1996), arXiv:nucl-th/9604032 [nucl-th].
- [37] V. A. Khodel, V. V. Khodel, and J. W. Clark, *Phys. Rev. Lett.* **81**, 3828 (1998), arXiv:nucl-th/9807034 [nucl-th].
- [38] M. Baldo, O. Elgaroy, L. Engvik, M. Hjorth-Jensen, and H. J. Schulze, *Phys. Rev. C* **58**, 1921 (1998), arXiv:nucl-th/9806097 [nucl-th].
- [39] V. V. Khodel, V. A. Khodel, and J. W. Clark, *Nucl. Phys.* **A679**, 827 (2001), arXiv:nucl-th/0001006 [nucl-th].
- [40] M. V. Zverev, J. W. Clark, and V. A. Khodel, *Nucl. Phys.* **A720**, 20 (2003), arXiv:nucl-th/0301028 [nucl-th].
- [41] S. Maurizio, J. W. Holt, and P. Finelli, *Phys. Rev. C* **90**, 044003 (2014), arXiv:1408.6281 [nucl-th].
- [42] S. K. Bogner, R. J. Furnstahl, and A. Schwenk, *Prog. Part. Nucl. Phys.* **65**, 94 (2010), arXiv:0912.3688 [nucl-th].
- [43] S. Srinivas and S. Ramanan, *Phys. Rev. C* **94**, 064303 (2016), arXiv:1606.09053 [nucl-th].
- [44] F. Tabakin, *Phys. Rev.* **174**, 1208 (1968).
- [45] M. Hoffberg, A. E. Glassgold, R. W. Richardson, and M. Ruderma, *Phys. Rev. Lett.* **24**, 775 (1970).
- [46] R. Tamagaki, *Progress of Theoretical Physics* **44**, 905 (1970), <https://academic.oup.com/ptp/article-pdf/44/4/905/5386708/44-4-905.pdf>.
- [47] T. Takatsuka and R. Tamagaki, *Progress of Theoretical Physics Supplement* **112**, 27 (1993), <https://academic.oup.com/ptps/article-pdf/doi/10.1143/PTP.112.27/5205856/112-27.pdf>.
- [48] T. Takatsuka, *Progress of Theoretical Physics* **47**, 1062 (1972), <https://academic.oup.com/ptp/article-pdf/47/3/1062/5443245/47-3-1062.pdf>.
- [49] R. W. Richardson, *Phys. Rev. D* **5**, 1883 (1972).
- [50] J. Sauls and J. Serene, *Phys. Rev. D* **17**, 1524 (1978).
- [51] K. Masuda and M. Nitta, *Phys. Rev. C* **93**, 035804 (2016), arXiv:1512.01946 [nucl-th].
- [52] S. Yasui, C. Chatterjee, and M. Nitta, *Phys. Rev. C* **99**, 035213 (2019), arXiv:1810.04901 [nucl-th].
- [53] S. Yasui, C. Chatterjee, M. Kobayashi, and M. Nitta, *Phys. Rev. C* **100**, 025204 (2019), arXiv:1904.11399 [nucl-th].
- [54] P. Muzikar, J. A. Sauls, and J. W. Serene, *Phys. Rev. D* **21**, 1494 (1980).
- [55] J. A. Sauls, D. L. Stein, and J. W. Serene, *Phys. Rev. D* **25**, 967 (1982).
- [56] K. Masuda and M. Nitta, *PTEP* **2020**, 013D01 (2020), arXiv:1602.07050 [nucl-th].
- [57] L. B. Leinson, *MNRAS* **498**, 304 (2020).
- [58] M. Kobayashi and M. Nitta, *Phys. Rev. C* **105**, 035807 (2022), arXiv:2203.09300 [nucl-th].
- [59] M. Kobayashi and M. Nitta, *Phys. Rev. C* **107**, 045801 (2023), arXiv:2209.07205 [nucl-th].
- [60] S. Yasui and M. Nitta, *Phys. Rev. C* **101**, 015207 (2020), arXiv:1907.12843 [nucl-th].
- [61] S. Yasui, C. Chatterjee, and M. Nitta, *Phys. Rev. C* **101**, 025204 (2020), arXiv:1905.13666 [nucl-th].
- [62] P. F. Bedaque, G. Rupak, and M. J. Savage, *Phys. Rev. C* **68**, 065802 (2003), arXiv:nucl-th/0305032 [nucl-th].
- [63] L. B. Leinson, *Phys. Lett.* **B702**, 422 (2011), arXiv:1107.4025 [nucl-th].
- [64] L. B. Leinson, *Phys. Rev. C* **85**, 065502 (2012), arXiv:1206.3648 [nucl-th].
- [65] L. B. Leinson, *Phys. Rev. C* **87**, 025501 (2013), arXiv:1301.5439 [nucl-th].
- [66] P. F. Bedaque and A. N. Nicholson, *Phys. Rev. C* **87**, 055807 (2013), [Erratum: *Phys. Rev. C* **89**, no.2, 029902(2014)], arXiv:1212.1122 [nucl-th].
- [67] P. Bedaque and S. Sen, *Phys. Rev. C* **89**, 035808 (2014).
- [68] P. F. Bedaque and S. Reddy, *Phys. Lett.* **B735**, 340 (2014), arXiv:1307.8183 [nucl-th].
- [69] P. F. Bedaque, A. N. Nicholson, and S. Sen, *Phys. Rev. C* **92**, 035809 (2015), arXiv:1408.5145 [nucl-th].
- [70] L. B. Leinson, *Phys. Rev. C* **81**, 025501 (2010), arXiv:0912.2164 [astro-ph.SR].
- [71] L. B. Leinson, *Phys. Lett.* **B689**, 60 (2010), arXiv:1001.2617 [astro-ph.SR].
- [72] L. B. Leinson, *Phys. Rev. C* **82**, 065503 (2010), arXiv:1012.5387 [hep-ph].
- [73] L. B. Leinson, *Phys. Rev. C* **83**, 055803 (2011), arXiv:1007.2803 [hep-ph].
- [74] L. B. Leinson, *Phys. Rev. C* **84**, 045501 (2011), arXiv:1110.2145 [nucl-th].
- [75] T. Mizushima, K. Masuda, and M. Nitta, *Phys. Rev. B* **95**, 140503 (2017), arXiv:1607.07266 [cond-mat.supr-con].
- [76] T. Mizushima, S. Yasui, and M. Nitta, *Phys. Rev. Res.* **2**, 013194 (2020), arXiv:1908.07944 [nucl-th].
- [77] T. Mizushima, S. Yasui, D. Inotani, and M. Nitta, *Phys. Rev. C* **104**, 045803 (2021), arXiv:2108.01256 [nucl-th].
- [78] Y. Masaki, T. Mizushima, and M. Nitta, *Phys. Rev. Res.* **2**, 013193 (2020), arXiv:1908.06215 [cond-mat.supr-con].
- [79] Y. Masaki, T. Mizushima, and M. Nitta, *Phys. Rev. B* **105**, L220503 (2022), arXiv:2107.02448 [cond-mat.supr-con].
- [80] Y. Masaki, T. Mizushima, and M. Nitta, in *Encyclopedia of Condensed Matter Physics (Second Edition)*, Vol. 2 (Elsevier, 2024) pp. 755–794, arXiv:2301.11614 [cond-mat.supr-con].
- [81] S. Yasui, D. Inotani, and M. Nitta, *Phys. Rev. C* **101**, 055806 (2020), arXiv:2002.05429 [nucl-th].
- [82] G. Marmorini, S. Yasui, and M. Nitta, *Sci. Rep.* **14**, 7857 (2024).
- [83] L. V. Drummond and A. Melatos, *MNRAS* **472**, 4851 (2017).

- [84] A. Sedrakian and P. B. Rau, *Phys. Rev. D* **111**, 023044 (2025), [arXiv:2407.13686 \[astro-ph.HE\]](#).
- [85] Y. Guo and H. Tajima, *Phys. Rev. B* **107**, 024511 (2023), [arXiv:2210.07042 \[cond-mat.quant-gas\]](#).
- [86] While the BdG formalism is valid in the whole temperature region, it is difficult to study dynamics of vortices that we are planning in a future work.
- [87] D. T. Son and M. A. Stephanov, *Phys. Rev. A* **65**, 063621 (2002), [arXiv:cond-mat/0103451](#).
- [88] K. Kasamatsu, M. Tsubota, and M. Ueda, *Phys. Rev. Lett.* **93**, 250406 (2004), [arXiv:cond-mat/0406150](#).
- [89] K. Kasamatsu, M. Tsubota, and M. Ueda, *Int. J. Mod. Phys. B* **19**, 1835 (2005), [arXiv:cond-mat/0505546](#).
- [90] M. Cipriani and M. Nitta, *Phys. Rev. Lett.* **111**, 170401 (2013), [arXiv:1303.2592 \[cond-mat.quant-gas\]](#).
- [91] M. Tylutki, L. P. Pitaevskii, A. Recati, and S. Stringari, *Phys. Rev. A* **93**, 043623 (2016), [arXiv:1601.03695 \[cond-mat.quant-gas\]](#).
- [92] M. Eto and M. Nitta, *Phys. Rev. A* **97**, 023613 (2018), [arXiv:1702.04892 \[cond-mat.quant-gas\]](#).
- [93] L. Calderaro, A. L. Fetter, P. Massignan, and P. Wittek, *Phys. Rev. A* **95**, 023605 (2017).
- [94] M. Eto, K. Ikeno, and M. Nitta, *Phys. Rev. Res.* **2**, 033373 (2020), [arXiv:1912.09014 \[cond-mat.quant-gas\]](#).
- [95] M. Kobayashi, M. Eto, and M. Nitta, *Phys. Rev. Lett.* **123**, 075303 (2019), [arXiv:1802.08763 \[cond-mat.stat-mech\]](#).
- [96] E. Babaev, *Phys. Rev. Lett.* **89**, 067001 (2002), [arXiv:cond-mat/0111192](#).
- [97] E. Babaev, *Nucl. Phys. B* **686**, 397 (2004), [arXiv:cond-mat/0201547](#).
- [98] E. Babaev, A. Sudbo, and N. W. Ashcroft, *Nature* **431**, 666 (2004), [arXiv:cond-mat/0410408](#).
- [99] J. Goryo, S. Soma, and H. Matsukawa, *EPL* **80**, 17002 (2007), [arXiv:cond-mat/0608015](#).
- [100] J. Garaud and E. Babaev, *Phys. Rev. B* **86**, 060514(R) (2012).
- [101] J. Garaud and E. Babaev, *Scientific Reports* **5**, 17540 (2015).
- [102] M. Nitta, M. Eto, T. Fujimori, and K. Ohashi, *J. Phys. Soc. Jap.* **81**, 084711 (2012), [arXiv:1011.2552 \[cond-mat.supr-con\]](#).
- [103] M. Eto and M. Nitta, *Phys. Rev. A* **85**, 053645 (2012), [arXiv:1201.0343 \[cond-mat.quant-gas\]](#).
- [104] M. Eto and M. Nitta, *EPL* **103**, 60006 (2013), [arXiv:1303.6048 \[cond-mat.quant-gas\]](#).
- [105] M. Nitta, M. Eto, and M. Cipriani, *J. Low Temp. Phys.* **175**, 177 (2013), [arXiv:1307.4312 \[cond-mat.quant-gas\]](#).
- [106] N. V. Orlova, P. Kuopanportti, and M. V. Milošević, *Phys. Rev. A* **94**, 023617 (2016).
- [107] D. S. Dantas, A. R. P. Lima, A. Chaves, C. A. S. Almeida, G. A. Farias, and M. V. Milošević, *Phys. Rev. A* **91**, 023630 (2015), [arXiv:1504.03203 \[cond-mat.quant-gas\]](#).
- [108] J. Garaud and E. Babaev, *Phys. Rev. B* **89**, 214507 (2014), [arXiv:1403.3373 \[cond-mat.supr-con\]](#).
- [109] C. Chatterjee, S. B. Gudnason, and M. Nitta, *Journal of High Energy Physics* **2020**, 10.1007/jhep04(2020)109 (2020).
- [110] Y. Kawaguchi and M. Ueda, *Physics Reports* **520**, 253 (2012).
- [111] M. Koashi and M. Ueda, *Phys. Rev. Lett.* **84**, 1066 (2000).
- [112] J. L. Song, G. W. Semenov, and F. Zhou, *Phys. Rev. Lett.* **98**, 160408 (2007), [arXiv:cond-mat/0702052](#).
- [113] S. Uchino, M. Kobayashi, M. Nitta, and M. Ueda, *Phys. Rev. Lett.* **105**, 230406 (2010), [arXiv:1010.2864 \[cond-mat.quant-gas\]](#).
- [114] M. Kobayashi and M. Nitta, *Phys. Rev. A* **104**, 053302 (2021).
- [115] M. Eto, K. Kasamatsu, M. Nitta, H. Takeuchi, and M. Tsubota, *Phys. Rev. A* **83**, 063603 (2011), [arXiv:1103.6144 \[cond-mat.quant-gas\]](#).
- [116] N. Hinohara, T. Oishi, and K. Yoshida, *Phys. Rev. C* **109**, 034302 (2024).
- [117] K. Yoshimura and K. Sekizawa, *Superfluid band theory for the rod phase in the magnetized inner crust matter: Entrainment, spin-orbit coupling, spin-triplet pairing* (2026), [arXiv:2601.13636 \[nucl-th\]](#).
- [118] E. Rydow, V. P. Singh, A. Beregi, E. Chang, L. Mathey, C. J. Foot, and S. Sunami, *Nat. Commun.* **16**, 7201 (2025).
- [119] L. Dominici, G. Dagvadorj, J. M. Fellows, D. Ballarini, M. De Giorgi, F. M. Marchetti, B. Piccirillo, L. Marrucci, A. Bramati, G. Gigli, M. H. Szymańska, and D. Sanvitto, *Sci. Adv.* **1**, e1500807 (2015).